Tetramerization of Phosphoprotein Is Essential for Respiratory Syncytial Virus Budding while Its N-Terminal Region Mediates Direct Interactions with the Matrix Protein

Monika Bajorek, Marie Galloux, Charles-Adrien Richard, Or Szekely, Rina Rosenzweig, Christina Sizun, Jean-François Éléouët

Tetramerization of Phosphoprotein is Essential for Respiratory Syncytial Virus Budding while its N Terminal Region Mediates Direct Interactions with the Matrix Protein.

Running title: Identification of P Protein Regions Interacting with M Protein

Monika Bajorek[a*], Marie Galloux[a], Charles-Adrien Richard[a], Or Szekely[b], Rina Rosenzweig[b], Christina Sizun[c*], Jean-Francois Eleouet[a]

[a]Université Paris-Saclay, INRAE, UVSQ, VIM, Jouy-en-Josas, France.
[b]Department of Structural Biology, Weizmann Institute of Science, Rehovot, Israel.
[c]Institut de Chimie des Substances Naturelles, CNRS, Université Paris-Saclay, Gif-sur-Yvette, France.

*Corresponding authors: email: monika.bajorek@inrae.fr; christina.sizun@cnrs.fr

Word count; Abstract: 170, Text: 8,003

Abstract

It was shown previously that the Matrix (M), Phosphoprotein (P), and the Fusion (F) proteins of Respiratory syncytial virus (RSV) are sufficient to produce virus-like particles (VLPs) that resemble the RSV infection-induced virions. However, the exact mechanism and interactions among the three proteins are not known. This work examines the interaction between P and M during RSV assembly and budding. We show that M interacts with P in the absence of other viral proteins in cells using a

Split Nano Luciferase assay. By using recombinant proteins, we demonstrate a direct interaction between M and P. By using Nuclear Magnetic Resonance (NMR) we identify three novel M interaction sites on P, namely site I in the α_{N2} region, site II in the 115-125 region, and the oligomerization domain (OD). We show that the OD, and likely the tetrameric structural organization of P, is required for virus-like filament formation and VLP release. Although sites I and II are not required for VLP formation, they appear to modulate P levels in RSV VLPs.

Importance

Human RSV is the leading cause of infantile bronchiolitis in the developed world and of childhood deaths in resource-poor settings. It is a major unmet target for vaccines and anti-viral drugs. The lack of knowledge of RSV budding mechanism presents a continuing challenge for VLP production for vaccine purpose. We show that direct interaction between P and M modulates RSV VLP budding. This further emphasizes P as a central regulator of RSV life cycle, as an essential actor for transcription and replication early during infection and as a mediator for assembly and budding in the later stages for virus production.

Introduction

Human RSV is the most frequent cause of infantile bronchiolitis and pneumonia worldwide (1). In France 460,000 infants are infected each year, of which ~30% develop lower respiratory infections and 4.8% to 6.7% are hospitalized, representing 45% of the young children admissions at the hospital (2). The enormous burden of RSV makes it a major unmet target for a vaccine and anti-viral drug therapy. However, despite over 60 years of research since its discovery, there is still no

vaccine available, and RSV therapy remains mainly supportive. The current standard of care consists of prophylactic treatment of at-risk infants with Palivizumab (Synagis), a monoclonal antibody. However, its limited efficacy (approximately 50%), and high cost (€5.000 per treatment) limits its use to pre-term infants. As a result, 60% of at risk children remain untreated, and no efficient therapy is available to treat the adult population (3). There are currently 39 vaccines under development (4). One of the strategies for RSV vaccine development is based on virus like particles (VLPs). However, all anti-RSV VLP vaccines currently in preclinical development are using foreign viral systems incorporating the RSV glycoproteins (5, 6). This is mostly due to the inefficiency of RSV VLP production (most of the virus is cell-associated in cell culture (7)), and to insufficient understanding of RSV particle assembly and budding. RSV VLPs, if they can be produced at sufficient levels, will accurately mimic the viral morphology and structure. Identification of the minimal players involved in particle assembly and budding is an important step in understanding the mechanism behind RSV particle formation. The knowledge can be then used for large scale VLPs and attenuated virus production for vaccination purpose.

RSV belongs to the *Pneumoviridae* family in the order *Mononegavirales* (8). It primarily infects epithelial cells of the respiratory tract and replicates in the cytoplasm. It is an enveloped, non-segmented, negative-strand RNA virus. The viral genome is encapsidated by the nucleoprotein (N), forming a ribonucleoprotein (RNP) complex, which constitutes the template for the viral polymerase. It was recently shown that the replication and transcription steps of RSV take place in virus-induced cytoplasmic inclusions called inclusion bodies (IBs), where all the proteins of the polymerase complex, i.e. the viral polymerase (L), its main co-factor the P protein,

the RNPs and the transcription factor M2-1 concentrate (9). It is noteworthy that pseudo-IBs, similar to those observed in RSV-infected cells, can be observed upon co-expression of only N and P (10, 11). We recently showed that the formation of these pseudo-IBs depends on a liquid-liquid phase separation induced by the N-P interaction (11). Once neo-synthesized, RNPs have to be exported from IBs to the plasma membrane, where RSV virions assemble and bud, forming elongated membrane filaments (12). According to the common paradigm, RSV assembles on the plasma membrane, and infectious viral particles are mainly filamentous (13, 14). However, recent data suggests that viral filaments are produced and loaded with genomic RNA prior to insertion into the plasma membrane. According to this model, vesicles with RSV glycoproteins recycle from the plasma membrane and merge with intracellular vesicles, called assembly granules, containing the RNPs (15, 16).

Regardless of the cellular location, the minimal RSV viral proteins required for efficient filament formation and budding of VLPs are P, M, and the F protein, more specifically its cytoplasmic tail (FCT) (17, 18). The atomic structure of the external part of F glycoprotein (excluding the transmembrane and cytoplasmic parts) has been resolved (19-21), but little is known about the FCT structure and its function in RSV assembly. M, a key structural protein, directs assembly and budding probably by interacting with FCT on the one hand, and with P associated to RNP on the other hand (22-24). M is required for filament elongation and maturation and, possibly, for transport of the RNP from IBs to the sites of budding (25). M was shown to localize to IBs where, presumably, the first interaction between M and the RNPs occurs. Some early reports have shown that M localization to IBs is mediated by interaction with M2-1 (26, 27). However, more recent work has demonstrated that M is found in

IBs when expressed with the N and P proteins alone (17). As N is not required for RSV virus-like filament formation, M was suggested to interact with P. However, the exact mechanism of interactions between these proteins remains largely unknown. Structural data published previously by our group showed that M forms dimers and that the switch from M dimers to higher order oligomers triggers assembly of viral filaments and virus production (28). Based on M structure, a long patch of positively charged surface spanning the entire monomeric protein was suggested to drive the interaction with a negatively-charged membrane (29).

Functional and structural data are available for the P protein, which is a multifunctional protein capable of interacting with multiple partners. Recent studies allowed better characterization of its interactions and functions within the viral polymerase complex. P forms tetramers of elongated shape composed of a central oligomerization domain (OD), mapped to residues N131-T151 (30-34), and of N- and C-terminal intrinsically disordered regions (IDRs). Structural study of P in solution by NMR gave insight into the secondary structure propensity of these IDRs, forming almost stable helices in the C-terminal region and extremely transient helices in the N-terminal region (35). Residues 1-29 in the N-terminal region confer a chaperone function to P, by binding monomeric and RNA-free N (N^0) and by maintaining N^0 unassembled (36). P C-terminal residues 232-241 were shown to bind RNA-bound N assembled as rings mimicking the RNP (37). Very recently, the structure of the L protein bound to tetrameric P solved by cryo-electron microscopy revealed that each of the four P monomers adopts a distinct conformation upon binding to L, the entire L-binding region on P spanning residues 130-228. This includes the OD and the major part of the C-terminal domain (32, 38, 39). As part of viral transcription

126 regulation, P region spanning residues 98-109 was shown to be the binding site for
127 the RSV transcription anti-termination factor M2-1 (40). This interaction is involved in
128 the recruitment of M2-1 to IBs (41). P also plays a pivotal role in M2-1 de-
129 phosphorylation mediated by the host protein PP1, which binds to P through an
130 RVxF-like motif located at P residues 82-87 (41). Dephosphorylated M2-1 is
131 recruited to specific regions in IBs, called IB associated granules (IBAGs), where
132 viral mRNAs are concentrated, before trafficking back to the cytoplasm. This cycle is
133 essential for RSV transcription and translation (41).
134
135 Recently, a P region encompassing residues 39–57 was found to be critical for VLP
136 formation (42). In this study it was also observed that the OD of P had no significant
137 contribution for VLP assembly and budding. Additionally, phosphomimetic
138 substitutions in P region 39-57 inhibited VLP formation, suggesting that this region
139 needs to be un-phosphorylated for VLP production (42). P region 110-120 was also
140 shown to be required for efficient virus budding, affecting the final step of filament
141 scission and virus release (42, 43). However, until now, no direct interaction between
142 P and M has been shown. The lack of structural information on the putative M-P
143 complex makes it difficult to speculate about the mechanism of budding. Thus,
144 identifying specific RSV M-P protein-protein interactions has the potential to break
145 new ground in our understanding of the mechanism behind RSV particle formation.
146 This can further benefit RSV VLP-based vaccine research.
147
148 **Results**
149 **Specific localization of M depends on expression of F, P, and N proteins.**

As shown previously, RSV VLPs can be generated independently of viral infection by transfecting cells with plasmids encoding the RSV M, P, N, and F proteins (18, 28). Although N is not required for RSV filament formation (17), it localizes with M in filaments when present, and is required, together with P, for the formation of pseudo-IBs (18, 28). In a first attempt to study the co-localization of M with N and P proteins in pseudo-IBs and in virus-like filaments at the plasma membrane, and to confirm the minimal requirement for filament formation in our system, we used a transfection-based assay.

BEAS-2B cells were transfected to express M, N, P, and F, or various combinations of these four proteins. The intracellular localization of RSV proteins and the formation of pseudo-IBs and virus-like filaments were determined by confocal imaging after staining in parallel with either anti-M and anti-N antibodies (Fig. 1A), or anti-P and anti-N (Fig. 1B). In the presence of M, N, P, and F, the formation of pseudo-IBs and of virus-like filaments was detected by immunostaining of M, N and P. Co-localization of M, N, and P was detected on filaments at the plasma membrane as well as in pseudo-IBs, as shown in zoomed merged images (Fig. 1A and 1B, row 1, positive control). When F was absent, M, P, and N localized in pseudo-IBs (Fig. 1A and 1B, row 2). M, but not P or N, was also found in small spikes, most probably at the plasma membrane. In the absence of P or N, no pseudo-IBs formed, as expected (Fig. 1A and 1B, rows 3 and 4). In the absence of P, M was found only as small spikes, whereas N spread all throughout the cytoplasm (Fig. 1A and 1B, row 3). Finally, as previously reported, large filaments containing M and P formed in the absence of N (Fig. 1A and 1B, row 4). Altogether, our results confirm previous observations showing that only M, P, and F are required for virus-

like filaments formation, and that M co-localizes with N and P within pseudo-IBs and in virus-like filaments (17, 18, 26, 28).

M interacts with P in cells

As M localization in virus-like filaments seems to depend on P, we then studied whether M can interact with P in cells in the absence of other viral proteins. For that purpose, we used the NanoLUC interaction assay based on the split Nano Luciferase reporter (44). In this system, the 114 or the 11S Nano Luciferase fragments were fused to the C-terminus of viral proteins (Fig. 2A). Analysis of the lysates of transfected 293T cells by Western blotting using anti-P, anti-M, anti-N or anti-M2-1 antibody, confirmed protein expression with the fused NanoLUC fragments (Fig. 2B). In addition to the expected bands, a weak higher migrating band, probably unspecific, was detected in P114 and P-11S samples, whereas a double band was detected in M2-1-11S sample, corresponding most probably to the phosphorylated and unphosphorylated forms of M2-1 (41).To investigate the P-M interaction, combinations of two constructs were transfected into 293T cells. 24 h post transfection cells were lysed, luciferase substrate was added, and the luminescence, proportional to the strength of the interaction, was measured (Fig. 2C). As P is known to form tetramers (30-35), P/P interaction was used as positive control. As shown in Fig. 2C, transfection of P-114/P-11S resulted in a high luminescence signal, indicating a strong interaction. We also used the P-N interaction as a control: when co-expressing P-114 and N-11S, positive but relatively low luminescence was observed. Here, as the NanoLUC 114 subunit was cloned at the C-terminus of P protein, thus blocking the interaction between the C-terminus of P and RNA-bound N, the luminescence signal corresponds to the P-N^0 interaction, which was

199 previously shown to be rather weak, in the micromolar range (36). When M-114 was
200 co-expressed with P-11S, the luminescence signal was similar to the P-N^0 signal,
201 suggesting that M interacts with P with similar affinity compared to P-N^0 interaction.
202 In contrast, expression of M-114 with M2-1-11S did not produce luminescence,
203 suggesting that M and M2-1 did not interact when co-expressed in cells in our
204 system. However, for this negative result, we cannot exclude that the C-terminal tag
205 blocks protein-protein interactions that occur via the C-terminus of one or both
206 proteins.
207
208 **M directly interacts with P via its N-terminal region and OD**
209 Next, we investigated whether M directly interacts with P *in vitro* using recombinant
210 proteins, and determined the P region involved in the interaction. Based on structural
211 data available for isolated P (30, 35), we generated rational deletions of each
212 subdomain of P (Fig. 3A). While P fragments lacking the OD ($P_{\Delta OD}$, P_{1-126} and P_{161-}
213 $_{241}$) were shown to be monomeric by NMR, P fragments containing the OD (full-
214 length P, P_{OD}, P_{1-163} and $P_{127-241}$) appeared to be associated via the OD (35). The
215 purity and the size of all the P fragments were controlled by SDS-PAGE (Fig. 3B). M
216 and full-length P or P fragments were co-incubated and the formation of complexes
217 was analysed by native agarose gel electrophoresis. Of note, in native gels proteins
218 migrate according to the combination of their size, shape and charges. This explain
219 why $P_{\Delta OD}$ migrates at higher apparent molecular weight than full-length P, as the
220 global charges are -20.7 for monomeric $P_{\Delta OD}$ and -86.8 for tetrameric P at pH 7.4.
221 When M was incubated with P fragments, shifts were observed only with full-length P
222 and P_{1-163} (Fig. 3C), indicating that the N-terminal domain of P (residues 1-131) and
223 the OD (residues 131-151) are together required for a stable P-M interaction in this

system. Additionally, no shift was observed neither for $P_{\Delta OD}$ nor for P_{1-126} when incubated in the presence of M. This suggests that either the M-binding site is at least partly on the OD of P, or that M interaction requires tetrameric P. Since no shift was observed for P_{OD}, $P_{127-241}$ and $P_{161-241}$ when incubated with M, these results showed that the OD or the C-terminal region of P on their own or together were not sufficient for a detectable P-M interaction *in vitro.*

Based on these results, we next wanted to assess if a P fragment containing the N-terminal region and the OD was sufficient to interact with M and to induce membrane filaments in cells. We used the P_{1-161} fragment, shorter than P_{1-163} by two residues, which are outside of the OD on the C-terminal side. Again, we used the filament formation assay. BEAS-2B cells were transfected to express M, N, F and P, P_{1-161} or P_{1-126} constructs, and the formation of RSV virus-like filaments was determined by confocal imaging after staining with anti-M and anti-P primary antibodies (Fig. 3D). As previously shown (Fig. 1), in the presence of M, N, F, and P, the formation of pseudo-IBs and virus-like filaments was observed, and M co-localized with P in both structures (Fig. 3D, row 1, positive control). Co-localization was not seen in all pseudo-IBs, but this could reflect different maturation states of pseudo-IBs. In the absence of P or when P_{1-126} was expressed, neither IBs nor virus-like filaments were detected, and M was found in small spikes (Fig 3D, row 2 and 4). Virus-like filaments were detected when the P_{1-161} construct was expressed, and M-P_{1-161} co-localization occurred in virus-like filaments (Fig 3D, row 3). These results are in agreement with those obtained with the gel shift assay using recombinant proteins (Fig. 3C), and confirmed that the P_{1-161} fragment is competent for M binding and for filament formation. It is noteworthy that under these conditions no pseudo-IBs were detected, because the interaction between the C-terminus of P (missing in the P_{1-161} construct)

and N is critical for their formation (45). Altogether, our results show that the P_{1-161} fragment is sufficient to interact with M and to induce the formation of virus-like filaments in cells in presence of M, N, and F.

Identification of M interaction sites on P by NMR

Next, we sought for a method to identify the M interaction site on P, in a residue–specific manner, without resorting to mutations or internal deletions in potential regions of interest. We have previously used NMR to localize molecular recognition features (MoRFs) on P, taking advantage of the intrinsically disordered nature of this protein (46). Perturbations in amide ^{1}H-^{15}N correlation spectra, either of intensities (Fig. 4A and 5) or chemical shifts, were used to map regions that sense direct interaction and/or conformational changes due to binding of a partner.

To control the oligomerization state of M, we used the M-Y229A mutant, which was shown to form dimers, but is less prone to form higher order oligomers as compared to WT M (28). No aggregation or self-assembly of M-Y229A was observed, as the samples stayed clear and M-specific signal was detected in ^{1}H NMR spectra, also in the presence of P (Fig. 4B). Of note, since M-Y229A is a dimeric 2x29 kDa folded protein, M signals are much broader than P signals that stem from the intrinsically disordered N-terminal region of P. This was also verified by SEC analysis made after NMR measurements (data not shown). A buffer with reduced ionic strength (150 mM NaCl as compared to 300 mM, the usual M storage buffer (13)) was used to enhance potential electrostatic interactions between M and P. The temperature was set to 288 K to increase the stability of M in this buffer, and also to reduce NMR signal broadening of solvent-exposed amide protons due to exchange with water. The final concentration of M was set to 100 µM. Concentrations and molar ratios are given for

274 protomers, independently of the oligomerization state of the proteins. Since the C-
275 terminal part of P seemed to be dispensable for interaction with M and for virus-like
276 filament formation (Fig. 3), we performed experiments with ^{15}N-labeled P fragments
277 devoid of this part rather than with full-length P: this reduces signal overlap in ^{1}H-^{15}N
278 correlation spectra.

279 Incubation of ^{15}N-labeled P_{1-163} with M-Y229A at a P:M molar ratio of 1:4 (25 µM P
280 and 100 µM M) resulted in significant intensity decrease of several P_{1-163} amide
281 signals in 2D ^{1}H-^{15}N correlation NMR spectra (Fig. 4A). These perturbations took
282 place in two proximal regions located immediately upstream of the OD: in the α_{N2}
283 region (residues 98-111) and in a stretch spanning residues 115-125 (Fig. 4C). The
284 first corresponds to the extremely transient helix α_{N2}, previously identified as the
285 binding site of RSV M2-1 protein (46, 47). Due to specific dynamics in the α-helical
286 coiled-coil OD, amide ^{1}H-^{15}N signals are broadened out beyond detection at 288 K
287 for P fragments that contain the OD flanked by N- and/or C-terminal extensions (46).
288 Hence, M-binding to the OD could not be assessed using P_{1-163}.

289 A concentration effect for P_{1-163} was evidenced by comparing the intensity ration I/I_0
290 measured with two different P:M molar ratios (Fig. 4C). A maximal effect, where
291 signals disappear completely, could not be reached, because M could not be
292 concentrated above 100 µM without starting to aggregate and because the
293 concentration of ^{15}N-labeled P had to be kept >10 µM due to the sensitivity limitation
294 of NMR. Altogether, the NMR experiments with P_{1-163} show that an interaction takes
295 place between P_{1-163} and M-Y229A, which involves a region immediately upstream of
296 the OD. This interaction is rather weak. A set of NMR data with P_{1-163} and M-Y229A
297 was also acquired in a buffer with 300 mM NaCl and compared to 150 mM NaCl
298 (Fig. 4D). Overall intensity perturbation is larger with lower salt concentration,

299 indicating that M-Y229A binding is stronger under these conditions and suggesting
300 that there may be an electrostatic contribution to the P-M interaction.
301 To assess the role of the OD, we used the P_{1-126} fragment, which is devoid of it.
302 When incubated with 4 molar equivalents of M-Y229A, no significant effect was
303 observed in the intensities of the ^{1}H-^{15}N correlation spectrum (Fig. 5A and 5D, upper
304 panel), indicating that the OD is required for M binding. These results correlate well
305 with the band shift experiments for the M/P complex using native gel analysis (Fig.
306 3C). To further characterize the binding site on P_{1-163}, we performed NMR
307 interactions experiments using the shorter $P_{113-163}$ fragment, which contains only the
308 OD flanked by residues 115-130 and 152-163 (Fig. 5B and 5D, lower panel). In the
309 presence of M-Y229A, NMR signal intensities decreased by 30 % upstream and
310 downstream of the OD. A stronger effect was again observed for residues 115-125
311 (Fig. 5B and 5D, lower panel), suggesting that they play a particular role in M
312 binding. Like for P_{1-163}, the OD could not be observed for $P_{113-163}$ fragment at 288 K.
313 However, these signals become visible at higher temperature for $P_{113-163}$ (Fig. 5B
314 and 5D, lower panel). The intensity perturbation pattern of $P_{113-163}$ at 298 K suggests
315 that the OD region is affected by the presence of M-Y229A. For $P_{120-160}$, the smallest
316 fragment used in this study, all amide signals can be observed, even at 288 K (Fig.
317 5C). M-Y229A induces a weak global reduction in intensity that may point to weak
318 binding to $P_{120-160}$. Taken together, these results suggest that M binding to P is
319 achieved through multiple contact sites that are located in α_{N2} (site I), in the 115-125
320 region (site II) and potentially in the OD. Binding to any of these sites appears be
321 rather weak, and M binding to the two N-terminal P regions requires tetrameric P.
322
323 **Validation of M-binding sites on P using P deletion mutants**

In order to validate the NMR data showing multiple M binding sites, we then performed band shift assays with different fragments of P. We generated P deletions using P_{1-163} as a template and deleted a different part of the N-terminal domain for each construct. The OD was present in all constructs to keep the P protein as a tetramer (Fig. 6A). Each construct contained different M-binding domains. P_{40-163} contained the region spanning residues 39-57, previously reported to affect RSV assembly and potentially being involved in M interaction (42), as well as all binding sites identified by NMR (Fig. 4 and 5). P_{80-163} contained the two potential binding sites I and II identified by NMR. $P_{113-163}$ contained only site II, and $P_{120-160}$ lacked both sites, containing only the OD. We used both WT M and M-Y229A in order to ascertain that the NMR results were not biased by the Y229A M mutation. M proteins, full-length P and P fragments were purified as previously and analysed by SDS-PAGE (Fig. 6B). M and P constructs were co-incubated before analysis of complexes by native agarose gel electrophoresis (Fig. 6C). Shifts were observed with full-length P and P_{1-163}, as shown above in Fig. 3C. P_{40-163} and P_{80-163} fragments (containing both sites I and II and OD) also induced a shift. No band shift was detected when M was incubated with $P_{113-163}$ (containing only site II and OD) or with $P_{120-160}$. Similar shifts were observed for M WT and M Y229A. This is in line with our NMR results (Fig. 4 and 5), indicating that M binding by P is achieved through multiple sites. Interactions seen by NMR with $P_{113-126}$ or $P_{120-160}$ were not strong enough to induce a band shift when analyzed by native gel electrophoresis.

In order to verify which of the identified specific M/P binding regions is relevant for interaction between M and P in cells, we used again the NanoLUC interaction assay based on the split Nano Luciferase reporter. The 114 or the 11S Nano Luciferase fragments were fused to the C-terminus of M and P proteins (Fig. 2A). P_{WT} and four

P deletion mutants were analysed: $P_{\Delta 39-57}$ (deleted of the region previously reported to be involved in M/P interaction (42)), $P_{\Delta 93-126}$ (lacking sites I and II as identified by NMR), $P_{\Delta 39-57,\Delta 93-126}$ (lacking the three regions), and $P_{\Delta OD}$. Combinations of two proteins were transfected into 293T cells. 24 h post transfection cells were lysed, luciferase substrate was added, and the luminescence, proportional to the strength of the interaction, was measured (Fig. 6D). P/P interaction was again used as positive control. As shown in Fig. 6D, transfection of P-114/P-11S resulted in high luminescence signal, indicating a strong interaction. Transfection of M-114 and P-11S resulted in positive signal (comparable to Fig. 2C). Transfection of $P_{\Delta 39-57}$-11S, $P_{\Delta 93-126}$-11S, or $P_{\Delta 39-57,\ \Delta 93-126}$-11S and M-114, all resulted in luminescence comparable to transfection when P-11S was used. In contrast, when M-114 was transfected with $P_{\Delta OD}$-11S, luminescence signal was almost completely lost. These results indicate that, in transfected cells, P OD deletion, and as a consequence abrogated tetramerization, resulted in a significant loss of interaction with M, whereas deletion of amino acids 39-57, 93-126 or both regions did not. Of note, analysis of the lysates of transfected 293T cells by Western blotting using anti-P or anti-M antibody confirmed correct protein expression with the fused NanoLUC fragments (Fig. 6E).

Functional implications of P regions displaying direct M-binding

Next, we asked whether the identified M-binding domains on P were of functional significance. We analysed virus-like filament formation using full-length P or deletion constructs based on NMR results and on previous publications. Specifically, we checked full-length P, P_{1-161}, $P_{\Delta OD}$, $P_{\Delta 39-57}$, $P_{\Delta 93-110}$ (deleted of M-binding site I), $P_{\Delta 113-126}$ (deleted of M-binding site II), and $P_{\Delta 93-126}$ (deleted of both sites I and II as

identified by NMR) (Fig. 7A). BEAS-2B cells were transfected to express M, N, F and P_{WT} or various P deletion constructs, and the formation of RSV virus-like filaments was determined by confocal imaging and immuno-fluorescence after staining with anti-M and anti-P primary antibodies (Fig. 7B). Transfecting M, N, F and P resulted in pseudo-IBs and filament formation, and co-localization of M and P proteins in both (positive control, Fig. 7B, upper left). Transfecting M, N, F and $P_{\Delta OD}$ did not produce any virus-like filaments or pseudo-IBs, and M and P did not co-localize (Fig. 7B, lower left). Cells expressing $P_{\Delta 39-57}$ failed to produce virus-like filaments, and although P was found in pseudo-IBs, M was not recruited to IBs (Fig. 7B, upper right). Transfection of $P_{\Delta 93-126}$ resulted in virus-like filament formation (Fig. 7B, lower right), and both M and P proteins were found in virus-like filaments, similar to P_{WT}, showing that sites I and II are not critical for these processes.

Finally, we asked whether P deletion mutants could negatively affect VLP release. HEp-2 cells were transfected to express M, F, and various P constructs. The N protein was not included in the assay, since it is not required for VLP production (Fig. 1 and (17)). Cell lysates (soluble fractions) and the VLPs released into the media were analysed by Western blotting using anti-P and anti-M antibodies (Fig. 7C, upper panel). All P mutants were correctly expressed and were well detected by the anti-P antibody, as shown by the bands in the cell lysates. Quantification of relative M and P levels in the VLPs, revealed by WB, is shown in Fig. 7C, lower panel. When P_{WT} was expressed, VLP release was validated using anti-M antibodies, and P was detected in VLPs using anti-P antibodies (positive control). The absence of P prevented VLP release (negative control). The P_{1-161} construct resulted in VLP release comparable to P_{WT}. Expression of $P_{\Delta OD}$ significantly reduced VLP release, as almost no M could be detected. $P_{\Delta 39-57}$ abolished VLP release, as no M and P were

399 detected. This is in agreement with our virus-like filament formation assay (Fig. 7B),
400 where neither $P_{\Delta OD}$ nor $P_{\Delta 39-57}$ induced filament formation. Transfection of $P_{\Delta 93-110}$,
401 $P_{\Delta 113-126}$ or $P_{\Delta 93-126}$ mutants did not abolish VLP release, as M was detected in the
402 VLP fraction at comparable levels to P_{WT} with $P_{\Delta 93-126}$, or slightly reduced with $P_{\Delta 93-}$
403 $_{110}$ and $P_{\Delta 113-126}$. $P_{\Delta 93-110}$ incorporation into released VLPs was comparable to that of
404 P_{1-161}, i.e. with only a 25-30% reduction relative to P_{WT}. In contrast, transfection of
405 $P_{\Delta 113-126}$ and even more of $P_{\Delta 93-126}$ significantly reduced detection of these mutants in
406 released VLPs. This suggests that $P_{\Delta 113-126}$ and $P_{\Delta 93-126}$ mutants still supported VLP
407 formation, in contrast to $P_{\Delta OD}$ and $P_{\Delta 39-57}$, but could be more easily displaced from
408 VLPs than $P_{\Delta 93-110}$, P_{1-161} or P_{WT}. This effect appears to be linked to the deletion of
409 site II. It was not evidenced in the virus-like filament formation assay carried out with
410 $P_{\Delta 93-126}$ (Fig. 7B), most likely because this assay examined filaments formation *in*
411 *situ*, rather than VLPs that underwent a purification process. Additionally, the
412 discrepancy can be attributed to the fact immunofluorescence method is not
413 quantitate and the difference in P levels was not detected.
414

415 **Discussion**

416 **RSV M makes a direct interaction with RSV P**

417 It was reported earlier that the three proteins, RSV P, M and F were sufficient for
418 virus-like filament formation and VLP release (17). Our results confirm this minimal
419 requirement (Fig. 1). A question that remained open was which interactions M
420 needed to be involved in to promote assembly and budding of viral particles. For
421 *Paramyxoviridae* it was shown that M proteins organize viral assembly by bridging
422 between the glycoproteins and the RNPs, and that specific M-N interactions were
423 required for the RNP to be packed into viral pseudo-particles (48). The interaction

424 between the RNP and M proteins occurs most probably first in IBs and/or assembly
425 granules (16), where M recruits the RNP, before they are transported to viral
426 filaments formed on the cellular membrane.
427 Here we showed that M co-localized with P in pseudo-IBs, which are formed when N
428 and P are present, as well as in virus-like filaments, even in the absence of N (Fig.
429 1). Our NanoLUC results showed that M could interact with P in the absence of other
430 viral proteins in cells (Fig. 2). Gel shift assays performed with purified recombinant M
431 and P fragments (Fig. 3C) confirmed M and P could directly interact. Moreover, our
432 data indicated that the P domain responsible for this M interaction was located in
433 fragment P_{1-163}, comprising the N terminal domain and the OD of P (Fig. 3C and Fig.
434 6C). When M was co-expressed with P_{1-161}, no pseudo-IBs were formed, as
435 expected, since P_{1-161} lacks the C-terminus of P needed for interaction with RNA-N
436 complexes and formation of IBs (11, 37, 45). However, virus-like filaments were
437 formed, where M and P_{1-161} co-localized. This argues against the requirement of
438 preliminary IB formation before virus-like filament assembly, as these were observed
439 in cells transfected with RSV M, P, and F only. Furthermore, an interaction between
440 RSV M and P strongly suggests that for RSV assembly, bridging between M and the
441 RNP might be mediated by P.
442
443 **P displays multiple direct contact sites for M**
444 According to our NMR data (Fig. 4 and 5), M binding to P could be achieved through
445 multiple contact sites that are located within three regions, α_{N2} region (site I), the
446 115-125 region (site II) and the OD (Fig. 5). It must be noted that NMR experiments
447 were carried out with the M-Y229A mutant, which stays dimeric in solution. The
448 interactions observed by NMR therefore represent a P-M complex formed with

449 dimeric M. The NMR results were corroborated *in vitro* by native gel interaction
450 assays using both M WT and M-Y229A and N-terminally truncated P fragments (Fig.
451 3 and 6). Interestingly, neither sites I and II together but without the OD ($P_{1–126}$ as
452 compared to $P_{80–163}$ or $P_{1–163}$) nor the OD without sites I and II ($P_{120–160}$ as compared
453 to $P_{80–163}$) seemed to be sufficient to bind M (Fig. 3C, 4, 5 and 6C). The split
454 luciferase assay shed another light on the complexity of M-P interactions. The
455 deletion of the internal N-terminal region spanning site I and II did not impair M
456 binding *in cellula*, in contrast to the internal deletion of the OD, which completely
457 impaired the M-P interaction under the same conditions (Fig. 6D). This could indicate
458 that other short intrinsically disordered N-terminal motifs, similar in sequence to sites
459 I or II, could complement the M-binding site, as they are closer to the OD than in P_{WT}
460 due the 30-residue long truncation, or that cellular proteins help stabilize the M-P
461 complex. Interestingly, as illustrated by the $P_{\Delta 39-57}$ deletion mutant, highlighting the
462 essential role of the 39-57 region (42), the ability to form an M-P complex *in cellula* is
463 not correlated with virus-like filament formation or P-M co-localization on these virus-
464 like filaments (Fig. 6D and 7B).
465 Although P OD is not sufficient to bind M, it seems to play a major role, possibly
466 because of the higher level of structural organization provided by tetramerization. We
467 previously showed that transient intra-protomer interactions take place in P (35), and
468 the cryo-EM structures of *Pneumoviridae* L-P complexes show that the four
469 protomers can engage each in different interaction in a single complex (32, 38, 39).
470 This suggests that the P-M interactions are complex and probably cooperative, and
471 that M could recognize one or several sites only formed when four P protomers are
472 present.

As can be seen from *Pneumoviridae* P protein sequence alignment (Fig. 8), the N-terminal P region contains conserved motifs, in particular the N^0-binding motif, the RVxF-like motif, which is the binding site for cellular PP1 phosphatase (41), and α_{N2}, which is the binding site for M2-1 protein. This region also contains conserved clusters of negatively charged residues, notably just upstream and inside binding site II. As indicated by reduced M-P binding in high salt buffer, these residues could be important for interaction with M, which displays a large positively charged surface patch (29). Finally, the differences observed between *in vitro* and *in cellula* experiments could also depend on post-translational modifications of the proteins.

Functional relevance of direct binding between M and P

Our virus-like filament formation and VLP assays shed light on the functional implications of these interactions. Whereas the OD, and likely tetrameric organization provided by the OD, was clearly needed for VLP formation, deletion of sites I or II individually, or both at the same time, did not prevent virus-like filament production (Fig. 7B). However, reduced levels of P were detected in released VLPs, when both sites I and II were simultaneously deleted (Fig. 7C). This could be attributed to detachment of mutated P from released VLPs during purification process or to defects in P incorporation when the final VLPs are formed rather than defective recruitment to virus-like filaments on plasma membrane, since these structures formed and co-localization between M and P was detected (Fig. 7B). This could also raise the question about the integrity of the VLPs that were still released.

M binding sites I and II thus rather appear to modulate P binding to M and to affect the final organization of the VLPs. The newly identified sites I and II also stand in contrast to the previously reported functional importance of the P region spanning

residues 39-57 (42). In agreement with previously published data, we confirm that $P_{\Delta 39-57}$ completely prevented filament formation and VLP budding (Fig. 7B and 7C). However, no perturbations were detected in the NMR signals in the 39-57 region of P in presence of M-Y229A (Fig. 4). The P-M interaction was still detected when residues 39-57 were deleted in transfected cells (Fig. 6D), indicating that this is probably not a direct binding region for M, at least not in its dimeric form. Dephosphorylation of the Ser/Thr-rich 39-57 region of P was reported to be required for VLP formation (42). This was the case for recombinant P protein produced in *E. coli*. As shown by our IF confocal microscopy experiments (Fig. 7B), M failed to co-localize to pseudo-IBs when $P_{\Delta 39-57}$ was expressed. This could indicate that a third, possibly cellular factor is required for M recruitment to IBs. Some early reports have shown that M localization to IBs was mediated by an interaction with M2-1 (26, 27), and M interaction with M2-1 in cells was shown by co-IP (49). Cryo-EM analysis of RSV filamentous particles showed that M2-1 is located between M layer and RNP (14, 50, 51). However, our work here shows that M2-1 is not required for M localization into pseudo-IBs (Fig. 1). Moreover M and M2-1 did not interact in our NanoLUC assay (Fig. 2).

In conclusion, our virus-like filament formation and VLP assays show a strong functional relevance of P region 39-57, which is essential for M localization to IBs and budding process, but most probably not due to a direct P-M binding. In addition, we show the functional importance of the tetramerisation of P, occurring via the short OD region. The OD is probably part of the M interaction site with P, but must be complemented by the N-terminal region of P to bind M (Fig. 7).

Possible role for RSV P as a switch between transcription and budding

523 Although the functional relevance of binding site I (α_{N2} region) could not be fully
524 assessed in the framework of this study, it is striking that it completely overlaps with
525 the binding site of transcription anti-termination factor M2-1, which is an essential
526 factor for efficient RSV transcription (52) (Fig. 8). It is likely that RNA synthesis
527 processes are frozen just before viral budding. However, such mechanism has not
528 been clearly investigated to our knowledge. It is established that P plays a critical
529 role in viral transcription, viral RNA synthesis and budding. In particular, interaction
530 of P with M2-1 is critical for M2-1 recruitment to IBs (53). The overlap of binding sites
531 for two essential proteins driving transcription (M2-1) on the one hand and virus
532 assembly (M) on the other hand, could be part of a switch mechanism, where both
533 proteins compete for this site. Interestingly, binding sites I and II contain four
534 reported phosphorylation sites on T108 (54), S116, S117 and S119 (43), which are
535 conserved among RSV P proteins (Fig. 8). Previously published data showed that P
536 phosphorylation on residue T108 abolished P-M2-1 interaction (54). Phosphomimetic
537 mutants of P serines 116, 117 and 119 (inside binding site II) were reported to
538 significantly prevent virus budding (43). Moreover, P lacking residues 110-120
539 reduced budding, which was completely restored when these residues were added
540 to P (42). P is known to be highly phosphorylated in purified virions, and the timing of
541 appearance of phosphorylated P was shown to correspond to the release of RSV
542 virions (55). We therefore suggest that the phosphorylation state of P sites I and II
543 could regulate the switch between RSV transcription/replication and assembly.
544 In summary, our work further confirms that RSV P protein is a multifunctional protein
545 playing different roles depending on its interactions with other viral proteins. We
546 confirm here that P plays a key role in RSV assembly. We also bring evidence for a

547 direct interaction between M and P, P OD being required for M-P interaction and
548 sites I and II modulating P binding to M in VLPs by mechanisms yet to uncover.
549
550 **MATERIALS AND METHODS**
551 **Plasmid constructs**
552 pcDNA3.1 codon-optimized plasmids for mammalian expression encoding the RSV
553 A2 M, P, N, F, and M2-1 proteins were a gift from Marty Moore, Emory University
554 (56). Commercially made pciNanoLUC 114 and 11S vectors (GeneCust) were used
555 to clone the RSV A2 codon-optimized M, P, N, and M2-1 constructs using standard
556 PCR, digestion and ligation techniques. pcDNA P_{1-126} and P_{1-161} deletion mutants of
557 P were obtained by introducing stop codons at the appropriate site in the coding
558 sequence. All pcDNA3.1 P deletion mutants in the full-length construct were
559 generated by using the Q5 site-directed mutagenesis kit (New England BioLabs),
560 following the manufacturer recommendations. pciNanoLUC 11S $P_{\Delta 39-57}$, $P_{\Delta 93-126}$, $P_{\Delta 39-}$
561 $_{57, \Delta 93-126,}$ and $P_{\Delta OD}$ mutants were obtained by re-cloning the relevant constructs from
562 pcDNA vector using standard PCR, digestion and ligation techniques. For
563 expression and purification of recombinant P proteins, the previously described
564 pGEX-P, and pGEX-P_{1-126}, pGEX-P_{1-163}, pGEX-$P_{\Delta OD}$, pGEX-$P_{127-241}$ and pGEX-$P_{161-241}$
565 plasmids were used (36). pGEX-P_{OD}, pGEX-P_{40-163}, pGEX-P_{80-163}, pGEX-$P_{113-163}$, and
566 pGEX-$P_{120-160}$ were generated using standard PCR, digestion and ligation techniques
567 and introducing codons at the appropriate site in the coding sequence. It is important
568 to note that pcDNA P_{1-161} and pGEX P_{1-163} were used for cellular expression or for
569 bacterial expression respectively. For expression and purification of recombinant M
570 protein, the previously described pCDF-M and pCDF-M_{Y229A} were used (28).
571

572 **Cell culture**

573 HEp-2 (ATCC CCL-23^{TM}) and 293T cells were maintained in Dulbecco modified
574 Eagle medium (eurobio) supplemented with 10% fetal calf serum (FCS; eurobio), 1%
575 L-glutamine, and 1 % penicillin streptomycin. The transformed human bronchial
576 epithelial cell line (BEAS-2B) (ATCC CRL-9609) was maintained in RPMI 1640
577 medium (eurobio) supplemented with 10% fetal calf serum (FCS; eurobio), 1% L-
578 glutamine, and 1% penicillin-streptomycin. The cells were grown at 37˚C in 5% CO2.

579

580 **Bacteria expression and purification of recombinant proteins**

581 For M expression (WT and Y229A mutant), *E. coli* Rosetta 2 bacteria transformed
582 with the pCDF-M plasmid were grown from fresh starter cultures in Luria-Bertani (LB)
583 broth for 5 h at 32°C, followed by induction with 0.4 mM isopropylthi-galactoside
584 (IPTG) for 4 h at 25°C. Cells were lysed by sonication (4 times for 20 s each time)
585 and lysozyme (1 mg/ml; Sigma) in 50 mM NaH_2PO_4-Na_2HPO_4, 300 mM NaCl, pH
586 7.4, plus protease inhibitors (Roche), RNase (12 g/ml, Sigma), and 0.25% CHAPS
587 {3-[(3-cholamidopropyl)-dimethylammonio]-1-propanesulfonate}, . Lysates were
588 clarified by centrifugation (23,425 g, 30 min, 4°C), and the soluble His_6-M protein
589 was purified on an Nickel sepharose column (HiTrap^{TM} 5 ml IMAC HP; GE
590 Healthcare). The bound protein was washed extensively with loading buffer plus 25
591 mM imidazole and eluted with a 25 to 250 mM imidazole gradient. M was
592 concentrated to 2 ml using Vivaspin20 columns (SartoriusStedimBiotec) and
593 purified on a HiLoad 10/600 Superdex S200 column (GE Healthcare) in 50 mM
594 NaH_2PO_4-Na_2HPO_4, 300 mM NaCl, pH 7.4. The M peak was concentrated to 3
595 mg/ml using Vivaspin4 columns. The quality of protein samples was assessed by
596 SDS-PAGE. Protein concentration was determined by measuring absorbance at 280

597 nm. For NMR interaction experiments a fresh preparation of M was dialyzed into
598 NMR buffer.
599 For P expression, *E.coli* BL21 (DE3) bacteria transformed with pGEX-P derived
600 plasmids were grown at 37˚C for 8 h in LB. Protein expression was induced by
601 adding one volume of fresh LB medium, 0.4 mM IPTG for 16 h at 28˚C. Bacterial
602 pellets were resuspended in lysis buffer (20 mM Tris/HCl pH 7.4, 60 mM NaCl, 1 mM
603 EDTA, 1 mg/mL lysozyme, 1 mM DTT, 0,1% Triton X-100) supplemented with
604 complete protease inhibitor cocktail (Roche) for 1 h on ice. Benzonase (Millipore)
605 was then added and the lysate was incubated for 1 h at RT under rotation. The
606 lysates were centrifuged at 4˚C for 30 min at 10,000g. Glutathione-Sepharose 4B
607 beads (GE Healthcare) were added to the clarified supernatants and the mixtures
608 were incubated overnight at 4˚C under rotation. The beads were washed with lysis
609 buffer, three times with 1X phosphate-buffered saline (PBS) and then stored at 4˚C
610 in an equal volume of PBS.
611 For ^{15}N-labeled P expression, bacteria were grown in minimal medium supplemented
612 with $^{15}NH_4Cl$ (Eurisotop) as a ^{15}N source. The GST tag was removed by thrombin
613 (Millipore) cleavage and the cleaved product exchanged into NMR buffer (50 mM Na
614 phosphate at pH 6.7, 150 mM NaCl). The quality of protein samples was assessed
615 by SDS-PAGE. Protein concentration was determined by Bradford assay (Biorad)
616 and checked by measuring absorbance at 280 nm for fragments containing tyrosine
617 residues. It is given as protomer concentration in the case of P tetramers.
618
619 **NanoLUC interaction assay**
620 Constructs expressing the NanoLUC subunits 114S and 11S were used (44). 293T
621 cells were seeded at a concentration of $3x10^4$ cells per well in 48-well plate. After 24

h, cells were co-transfected in triplicate with 0.4 µg of total DNA (0.2 µg of each plasmid) using Lipofectamine 2000 (Invitrogen). 24 h post transfection cells were washed with PBS, and lysed for 1 h in room temperature using 50 µl NanoLUC lysis buffer (Promega). NanoLUC enzymatic activity was measured using the NanoLUC substrate (Promega). For each pair of plasmids, three normalized luminescence ratios (NLRs) were calculated as follows: the luminescence activity measured in cells transfected with the two plasmids (each viral protein fused to a different NanoLUC subunit) was divided by the sum of the luminescence activities measured in both control samples (each NanoLUC fused viral protein transfected with an plasmid expressing only the NanoLUC subunit) Data represents the mean ±SD of 4 independent experiments, each done in triplicate. Luminescence was measured using Infinite 200 Pro (Tecan, Männedorf, Switzerland).

NMR spectroscopy

For NMR experiments, P and M solutions were mixed to obtain the desired molar ratio and concentrated to reach a concentration of 100 µM for M (WT and Y229A mutant).

NMR measurements were carried out in a Bruker Avance III spectrometer at a magnetic field of 18.8 T (800 MHz ^{1}H frequency) equipped with a cryogenic TCI probe. The magnetic field was locked with 7 % $^{2}H_2O$. The temperature was set to 288 K or 298 K. ^{1}H-^{15}N correlation spectra were acquired with a BEST-TROSY version. Spectra were processed with Topspin 4.0 (Bruker Biospin) and analyzed with CCPNMR 2.4 (57) software.

^{1}H and ^{15}N amide chemical shift assignment of full-length P and P_{1-126} and P_{1-163} fragments was done previously (46). Amide chemical shift assignment of ^{15}N-labeled

$P_{113-160}$ and of ^{15}N-labeled $P_{120-160}$ was done by recording a ^{15}N-separated NOESY-HSQC spectrum with 80 ms mixing time. Sequential information was retrieved through H_{Ni}-H_{Ni-1},H_{Ni}-H_{Ni+1} and H_{Ni}-$H_{\alpha i-1}$ correlations.

Virus-like filament/particle formation

Over night cultures of BEAS-2B cells seeded at 4 10^5 cells/well in 6-well plates (on a 16-mm micro-cover glass for immunostaining) were transfected with pcDNA3.1 codon-optimized plasmids (0.4 µg each) carrying the RSV A2 WT or deletion/mutant P protein along with pcDNA3.1 codon-optimized plasmids carrying RSV A2 M, N, and F using Lipofectamine 2000 (Invitrogen) according to the manufacturer's recommendations. Cells were fixed at 24 h post transfection, immunostained, and imaged as described below. For VLP formation, over-night cultures of HEp-2 cells seeded at 4 10^5 cells/well in 6-well plates were transfected as described above. Released VLPs were harvested from the supernatant; the supernatant was clarified of cell debris by centrifugation (1,300 g, 10 min, 4°C) and pelleted through a 20% sucrose cushion (13,500 g, 90 min, 4°C). Cells were lysed in radio immune precipitation assay (RIPA) buffer. Cellular lysates and VLP pellets were dissolved in Laemmli buffer and subjected to Western analysis.

Immunostaining and imaging

Cells were fixed with 4% paraformaldehyde in PBS for 10 min, blocked with 3% BSA in 0.2% Triton X-100–PBS for 10 min, and immunostained with monoclonal anti-M (1:200; a gift from Mariethe Ehnlund, Karolinska Institute, Sweden), polyclonal anti-N (1:5000; (30)), polyclonal anti-P (1:500; (30)) or monoclonal anti-P (1:100; a gift from Jose A. Melero, Madrid, Spain) antibodies, followed by species-specific secondary

antibodies conjugated to Alexa Fluor 488 and Alexa Fluor 568 (1: 1,000; Invitrogen). Images were obtained using the White Light laser SP8 (Leica Microsystems, Wetzlar, Germany) confocal microscope at a nominal magnification of 63. Images were acquired using the Leica Application Suite X (LAS X) software.

SDS-PAGE and Western analysis

Protein samples were separated by electrophoresis on 12% polyacrylamide gels in Tris-glycine buffer. All samples were boiled for 3 min prior to electrophoresis. Proteins were then transferred to a nitrocellulose membrane (RocheDiagnostics). The blots were blocked with 5% non fat milk in Tris-buffered saline (pH 7.4), followed by incubation with rabbit anti-P antiserum (1:5,000) (30), rabbit anti N antiserum (1:5,000) (30), rabbit anti M antiserum (1:1,000), or rabbit anti M2-1 antiserum (1:2,000) (30), and horseradish peroxidase (HRP)-conjugated donkey anti-rabbit (1:5,000) antibodies (P.A.R.I.S.). Western blots were developed using freshly prepared chemiluminescent substrate (100 mM TrisHCl, pH 8.8, 1.25 mM luminol, 0.2 mM p-coumaric acid, 0.05% H_2O_2) and exposed using BIO-RAD ChemiDoc™ Touch Imaging System.

Generation of M antiserum

Polyclonal anti M serum was prepared by immunizing a rabbit three times at 2 week intervals using purified His- fusion proteins (100 mg) for each immunization. The first and second immunizations were administered subcutaneously in 1 ml Freund's complete and Freund's incomplete adjuvant (Difco), respectively. The third immunization was done intramuscularly in Freund's incomplete adjuvant. Animals were bled 10 days after the third immunization.

Native gel

Protein samples were separated by electrophoresis on 1% agarose gel in TBE (Tris Borate EDTA) buffer. 50 µg M and x 10 µg P were incubated in PBS buffer (pH 7.4) for 20 min in RT. Samples were mixed with 50% sucrose and run for 2 h at 80 V, following by staining with Amido Black.

Acknowledgements

We thank Benoit Maury and CYMAGES Imaging facility (Département biotechnologie Santé, Université Versailles Saint Quentin, France) for their support & assistance with the confocal imaging. We thank Damien Vitour (E'quipe du laboratoire d'immunologie de Seppic and the animal facilities, ANSES Maisons-Alfort) for rabbit immunization with recombinant M. This work was carried out with the financial support of the French Agence Nationale de la Recherche DecRisP (ANR-19_CE11_0017).

References

1. Group TPERfCHPS. 2019. Causes of severe pneumonia requiring hospital admission in children without HIV infection from Africa and Asia: the PERCH multi-country case-control study. Lancet 394:757-79.
2. Grimprel E. 2001. [Epidemiology of infant bronchiolitis in France]. Arch Pediatr 8 Suppl 1:83S-92S.
3. Olszewska W, Openshaw P. 2009. Emerging drugs for respiratory syncytial virus infection. Expert Opin Emerg Drugs 14:207-17.
4. Mazur NI, Higgins D, Nunes MC, Melero JA, Langedijk AC, Horsley N, Buchholz UJ, Openshaw PJ, McLellan JS, Englund JA, Mejias A, Karron RA, Simoes EA, Knezevic I, Ramilo O, Piedra PA, Chu HY, Falsey AR, Nair H, Kragten-Tabatabaie L, Greenough A, Baraldi E, Papadopoulos NG, Vekemans J, Polack FP, Powell M, Satav A, Walsh EE, Stein RT, Graham BS, Bont LJ. 2018. The respiratory syncytial virus vaccine landscape: lessons from the graveyard and promising candidates. Lancet Infect Dis 18:e295-e311.
5. Schmidt MR, McGinnes-Cullen LW, Kenward SA, Willems KN, Woodland RT, Morrison TG. 2014. Modification of the respiratory syncytial virus f protein in virus-like particles impacts generation of B cell memory. J Virol 88:10165-76.
6. Lee YN, Hwang HS, Kim MC, Lee YT, Lee JS, Moore ML, Kang SM. 2015. Recombinant influenza virus expressing a fusion protein neutralizing epitope of respiratory syncytial virus (RSV) confers protection without vaccine-enhanced RSV disease. Antiviral Res 115:1-8.
7. Bachi T, Howe C. 1973. Morphogenesis and ultrastructure of respiratory syncytial virus. J Virol 12:1173-80.

8. Afonso CL, Amarasinghe GK, Banyai K, Bao Y, Basler CF, Bavari S, Bejerman N, Blasdell KR, Briand FX, Briese T, Bukreyev A, Calisher CH, Chandran K, Cheng J, Clawson AN, Collins PL, Dietzgen RG, Dolnik O, Domier LL, Durrwald R, Dye JM, Easton AJ, Ebihara H, Farkas SL, Freitas-Astua J, Formenty P, Fouchier RA, Fu Y, Ghedin E, Goodin MM, Hewson R, Horie M, Hyndman TH, Jiang D, Kitajima EW, Kobinger GP, Kondo H, Kurath G, Lamb RA, Lenardon S, Leroy EM, Li CX, Lin XD, Liu L, Longdon B, Marton S, Maisner A, Muhlberger E, Netesov SV, Nowotny N, et al. 2016. Taxonomy of the order Mononegavirales: update 2016. Arch Virol 161:2351-60.
9. Rincheval V, Lelek M, Gault E, Bouillier C, Sitterlin D, Blouquit-Laye S, Galloux M, Zimmer C, Eleouet JF, Rameix-Welti MA. 2017. Functional organization of cytoplasmic inclusion bodies in cells infected by respiratory syncytial virus. Nat Commun 8:563.
10. Garcia J, Garcia-Barreno B, Vivo A, Melero JA. 1993. Cytoplasmic inclusions of respiratory syncytial virus-infected cells: formation of inclusion bodies in transfected cells that coexpress the nucleoprotein, the phosphoprotein, and the 22K protein. Virology 195:243-7.
11. Galloux M, Risso-Ballester J, Richard CA, Fix J, Rameix-Welti MA, Eleouet JF. 2020. Minimal Elements Required for the Formation of Respiratory Syncytial Virus Cytoplasmic Inclusion Bodies In Vivo and In Vitro. MBio 11.
12. Roberts SR, Compans RW, Wertz GW. 1995. Respiratory syncytial virus matures at the apical surfaces of polarized epithelial cells. J Virol 69:2667-73.
13. Bajorek M, Caly L, Tran KC, Maertens GN, Tripp RA, Bacharach E, Teng MN, Ghildyal R, Jans DA. 2014. The Thr205 phosphorylation site within respiratory syncytial virus matrix (M) protein modulates M oligomerization and virus production. J Virol 88:6380-93.
14. Ke Z, Dillard RS, Chirkova T, Leon F, Stobart CC, Hampton CM, Strauss JD, Rajan D, Rostad CA, Taylor JV, Yi H, Shah R, Jin M, Hartert TV, Peebles RS, Jr., Graham BS, Moore ML, Anderson LJ, Wright ER. 2018. The Morphology and Assembly of Respiratory Syncytial Virus Revealed by Cryo-Electron Tomography. Viruses 10.
15. Vanover D, Smith DV, Blanchard EL, Alonas E, Kirschman JL, Lifland AW, Zurla C, Santangelo PJ. 2017. RSV glycoprotein and genomic RNA dynamics reveal filament assembly prior to the plasma membrane. Nat Commun 8:667.
16. Blanchard EL, Braun MR, Lifland AW, Ludeke B, Noton SL, Vanover D, Zurla C, Fearns R, Santangelo PJ. 2020. Polymerase-tagged respiratory syncytial virus reveals a dynamic rearrangement of the ribonucleocapsid complex during infection. PLoS Pathog 16:e1008987.
17. Meshram CD, Baviskar PS, Ognibene CM, Oomens AG. 2016. The Respiratory Syncytial Virus Phosphoprotein, Matrix Protein, and Fusion Protein Carboxy-Terminal Domain Drive Efficient Filamentous Virus-Like Particle Formation. J Virol 90:10612-10628.
18. Shaikh FY, Cox RG, Lifland AW, Hotard AL, Williams JV, Moore ML, Santangelo PJ, Crowe JE, Jr. 2012. A critical phenylalanine residue in the respiratory syncytial virus fusion protein cytoplasmic tail mediates assembly of internal viral proteins into viral filaments and particles. MBio 3.
19. McLellan JS, Chen M, Leung S, Graepel KW, Du X, Yang Y, Zhou T, Baxa U, Yasuda E, Beaumont T, Kumar A, Modjarrad K, Zheng Z, Zhao M, Xia N, Kwong PD, Graham BS. 2013. Structure of RSV fusion glycoprotein trimer bound to a prefusion-specific neutralizing antibody. Science 340:1113-7.
20. McLellan JS, Yang Y, Graham BS, Kwong PD. 2011. Structure of respiratory syncytial virus fusion glycoprotein in the postfusion conformation reveals preservation of neutralizing epitopes. J Virol 85:7788-96.
21. Swanson KA, Settembre EC, Shaw CA, Dey AK, Rappuoli R, Mandl CW, Dormitzer PR, Carfi A. 2011. Structural basis for immunization with postfusion respiratory syncytial virus fusion F glycoprotein (RSV F) to elicit high neutralizing antibody titers. Proc Natl Acad Sci U S A 108:9619-24.
22. Ghildyal R, Ho A, Jans DA. 2006. Central role of the respiratory syncytial virus matrix protein in infection. FEMS Microbiol Rev 30:692-705.
23. Kiss G, Chen X, Brindley MA, Campbell P, Afonso CL, Ke Z, Holl JM, Guerrero-Ferreira RC, Byrd-Leotis LA, Steel J, Steinhauer DA, Plemper RK, Kelly DF, Spearman PW, Wright ER. 2014. Capturing enveloped viruses on affinity grids for downstream cryo-electron microscopy applications. Microsc Microanal 20:164-74.
24. Harrison MS, Sakaguchi T, Schmitt AP. 2010. Paramyxovirus assembly and budding: building particles that transmit infections. Int J Biochem Cell Biol 42:1416-29.
25. Mitra R, Baviskar P, Duncan-Decocq RR, Patel D, Oomens AG. 2012. The human respiratory syncytial virus matrix protein is required for maturation of viral filaments. J Virol 86:4432-43.
26. Ghildyal R, Mills J, Murray M, Vardaxis N, Meanger J. 2002. Respiratory syncytial virus matrix protein associates with nucleocapsids in infected cells. J Gen Virol 83:753-7.
27. Li D, Jans DA, Bardin PG, Meanger J, Mills J, Ghildyal R. 2008. Association of respiratory syncytial virus M protein with viral nucleocapsids is mediated by the M2-1 protein. J Virol 82:8863-70.

28. Forster A, Maertens GN, Farrell PJ, Bajorek M. 2015. Dimerization of matrix protein is required for budding of respiratory syncytial virus. J Virol 89:4624-35.
29. Money VA, McPhee HK, Mosely JA, Sanderson JM, Yeo RP. 2009. Surface features of a Mononegavirales matrix protein indicate sites of membrane interaction. Proc Natl Acad Sci U S A 106:4441-6.
30. Castagne N, Barbier A, Bernard J, Rezaei H, Huet JC, Henry C, Da Costa B, Eleouet JF. 2004. Biochemical characterization of the respiratory syncytial virus P-P and P-N protein complexes and localization of the P protein oligomerization domain. J Gen Virol 85:1643-53.
31. Llorente MT, Taylor IA, Lopez-Vinas E, Gomez-Puertas P, Calder LJ, Garcia-Barreno B, Melero JA. 2008. Structural properties of the human respiratory syncytial virus P protein: evidence for an elongated homotetrameric molecule that is the smallest orthologue within the family of paramyxovirus polymerase cofactors. Proteins 72:946-58.
32. Gilman MSA, Liu C, Fung A, Behera I, Jordan P, Rigaux P, Ysebaert N, Tcherniuk S, Sourimant J, Eleouet JF, Sutto-Ortiz P, Decroly E, Roymans D, Jin Z, McLellan JS. 2019. Structure of the Respiratory Syncytial Virus Polymerase Complex. Cell 179:193-204 e14.
33. Simabuco FM, Asara JM, Guerrero MC, Libermann TA, Zerbini LF, Ventura AM. 2011. Structural analysis of human respiratory syncytial virus p protein: identification of intrinsically disordered domains. Braz J Microbiol 42:340-5.
34. Noval MG, Esperante SA, Molina IG, Chemes LB, Prat-Gay G. 2016. Intrinsic Disorder to Order Transitions in the Scaffold Phosphoprotein P from the Respiratory Syncytial Virus RNA Polymerase Complex. Biochemistry 55:1441-54.
35. Pereira N, Cardone C, Lassoued S, Galloux M, Fix J, Assrir N, Lescop E, Bontems F, Eleouet JF, Sizun C. 2017. New Insights into Structural Disorder in Human Respiratory Syncytial Virus Phosphoprotein and Implications for Binding of Protein Partners. J Biol Chem 292:2120-2131.
36. Galloux M, Gabiane G, Sourimant J, Richard CA, England P, Moudjou M, Aumont-Nicaise M, Fix J, Rameix-Welti MA, Eleouet JF. 2015. Identification and characterization of the binding site of the respiratory syncytial virus phosphoprotein to RNA-free nucleoprotein. J Virol 89:3484-96.
37. Tran TL, Castagne N, Bhella D, Varela PF, Bernard J, Chilmonczyk S, Berkenkamp S, Benhamo V, Grznarova K, Grosclaude J, Nespoulos C, Rey FA, Eleouet JF. 2007. The nine C-terminal amino acids of the respiratory syncytial virus protein P are necessary and sufficient for binding to ribonucleoprotein complexes in which six ribonucleotides are contacted per N protein protomer. J Gen Virol 88:196-206.
38. Sourimant J, Rameix-Welti MA, Gaillard AL, Chevret D, Galloux M, Gault E, Eleouet JF. 2015. Fine mapping and characterization of the L-polymerase-binding domain of the respiratory syncytial virus phosphoprotein. J Virol 89:4421-33.
39. Cao D, Gao Y, Roesler C, Rice S, D'Cunha P, Zhuang L, Slack J, Domke M, Antonova A, Romanelli S, Keating S, Forero G, Juneja P, Liang B. 2020. Cryo-EM structure of the respiratory syncytial virus RNA polymerase. Nat Commun 11:368.
40. Selvaraj M, Yegambaram K, Todd E, Richard CA, Dods RL, Pangratiou GM, Trinh CH, Moul SL, Murphy JC, Mankouri J, Eleouet JF, Barr JN, Edwards TA. 2018. The Structure of the Human Respiratory Syncytial Virus M2-1 Protein Bound to the Interaction Domain of the Phosphoprotein P Defines the Orientation of the Complex. MBio 9.
41. Richard CA, Rincheval V, Lassoued S, Fix J, Cardone C, Esneau C, Nekhai S, Galloux M, Rameix-Welti MA, Sizun C, Eleouet JF. 2018. RSV hijacks cellular protein phosphatase 1 to regulate M2-1 phosphorylation and viral transcription. PLoS Pathog 14:e1006920.
42. Meshram CD, Oomens AGP. 2019. Identification of a human respiratory syncytial virus phosphoprotein domain required for virus-like-particle formation. Virology 532:48-54.
43. Lu B, Ma CH, Brazas R, Jin H. 2002. The major phosphorylation sites of the respiratory syncytial virus phosphoprotein are dispensable for virus replication in vitro. J Virol 76:10776-84.
44. Dixon AS, Schwinn MK, Hall MP, Zimmerman K, Otto P, Lubben TH, Butler BL, Binkowski BF, Machleidt T, Kirkland TA, Wood MG, Eggers CT, Encell LP, Wood KV. 2016. NanoLuc Complementation Reporter Optimized for Accurate Measurement of Protein Interactions in Cells. ACS Chem Biol 11:400-8.
45. Galloux M, Tarus B, Blazevic I, Fix J, Duquerroy S, Eleouet JF. 2012. Characterization of a viral phosphoprotein binding site on the surface of the respiratory syncytial nucleoprotein. J Virol 86:8375-87.
46. Pereira N, Cardone C, Lassoued S, Galloux M, Fix J, Assrir N, Lescop E, Bontems F, Eleouet JF, Sizun C. 2017. New Insights into Structural Disorder in Human Respiratory Syncytial Virus Phosphoprotein and Implications for Binding of Protein Partners. The Journal of biological chemistry 292:2120-2131.
47. Richard CA, Rincheval V, Lassoued S, Fix J, Cardone C, Esneau C, Nekhai S, Galloux M, Rameix-Welti MA, Sizun C, Eleouet JF. 2018. RSV hijacks cellular protein phosphatase 1 to regulate M2-1 phosphorylation and viral transcription. PLoS Pathogens 14:e1006920.

48. Ray G, Schmitt PT, Schmitt AP. 2016. C-Terminal DxD-Containing Sequences within Paramyxovirus Nucleocapsid Proteins Determine Matrix Protein Compatibility and Can Direct Foreign Proteins into Budding Particles. J Virol 90:3650-60.
49. Kipper S, Hamad S, Caly L, Avrahami D, Bacharach E, Jans DA, Gerber D, Bajorek M. 2015. New host factors important for respiratory syncytial virus (RSV) replication revealed by a novel microfluidics screen for interactors of matrix (M) protein. Mol Cell Proteomics 14:532-43.
50. Kiss G, Holl JM, Williams GM, Alonas E, Vanover D, Lifland AW, Gudheti M, Guerrero-Ferreira RC, Nair V, Yi H, Graham BS, Santangelo PJ, Wright ER. 2014. Structural analysis of respiratory syncytial virus reveals the position of M2-1 between the matrix protein and the ribonucleoprotein complex. J Virol 88:7602-17.
51. Liljeroos L, Krzyzaniak MA, Helenius A, Butcher SJ. 2013. Architecture of respiratory syncytial virus revealed by electron cryotomography. Proc Natl Acad Sci U S A 110:11133-8.
52. Fearns R, Collins PL. 1999. Role of the M2-1 transcription antitermination protein of respiratory syncytial virus in sequential transcription. J Virol 73:5852-64.
53. Blondot ML, Dubosclard V, Fix J, Lassoued S, Aumont-Nicaise M, Bontems F, Eleouet JF, Sizun C. 2012. Structure and functional analysis of the RNA- and viral phosphoprotein-binding domain of respiratory syncytial virus M2-1 protein. PLoS Pathog 8:e1002734.
54. Asenjo A, Calvo E, Villanueva N. 2006. Phosphorylation of human respiratory syncytial virus P protein at threonine 108 controls its interaction with the M2-1 protein in the viral RNA polymerase complex. J Gen Virol 87:3637-42.
55. Lambert DM, Hambor J, Diebold M, Galinski B. 1988. Kinetics of synthesis and phosphorylation of respiratory syncytial virus polypeptides. J Gen Virol 69 (Pt 2):313-23.
56. Hotard AL, Shaikh FY, Lee S, Yan D, Teng MN, Plemper RK, Crowe JE, Jr., Moore ML. 2012. A stabilized respiratory syncytial virus reverse genetics system amenable to recombination-mediated mutagenesis. Virology 434:129-36.
57. Vranken WF, Boucher W, Stevens TJ, Fogh RH, Pajon A, Llinas M, Ulrich EL, Markley JL, Ionides J, Laue ED. 2005. The CCPN data model for NMR spectroscopy: development of a software pipeline. Proteins 59:687-96.
58. Notredame C, Higgins DG, Heringa J. 2000. T-Coffee: A novel method for fast and accurate multiple sequence alignment. J Mol Biol 302:205-17.
59. Pan J, Qian X, Lattmann S, El Sahili A, Yeo TH, Jia H, Cressey T, Ludeke B, Noton S, Kalocsay M, Fearns R, Lescar J. 2020. Structure of the human metapneumovirus polymerase phosphoprotein complex. Nature 577:275-279.

Figure legends

Fig.1: Specific localization of M depends on expression of F, P, and N proteins. BEAS-2B cells were co-transfected with pcDNA3.1 plasmids expressing RSV M, P, N, and F or a different combination of three proteins. 24 h post-transfection, cells were fixed, and immunostained with (**A)** anti-M (green) and anti-N (red) or (**B)** anti-P (green) and anti-N (red) primary antibodies followed by Alexa Fluor secondary antibodies, and were analyzed by confocal microscopy**.** Scale bars represent 10µm. Merged images are zoomed in 3X.

904 **Fig. 2: M interacts with P in cells.** Protein-protein interactions were measured
905 using the NanoLuc assay. **(A)** Scheme of the RSV protein constructs fused with
906 NanoLUC 114 or 11S subunit and pair combinations used in (C). **(B)** 293T cells were
907 transfected with plasmids encoding P, N, M, or M2-1 fused to 114 or 11S NanoLUC
908 subunit. Cells were lysed 24 h post transfection, and cell lysates were then subjected
909 to Western analysis using anti-P, anti-M, anti-N or anti-M2-1 polyclonal antibody.
910 Size markers are shown on the left side of each gel. **(C)** 293T cells were transfected
911 with pairs of constructs, combined as shown in the graph. P/P and P/N were used as
912 positive controls. Cells were lysed 24 h post transfection, and luminescence was
913 measured using a Tecan Infinite 200 plate reader. The NLR is the ratio between
914 actual read and negative controls (each protein with the empty NanoLUC vector).
915 The graph is representative of four independent experiments, each done in three
916 technical repeats. Data represents the means and error bars represent standard
917 deviation across 4 independent biological replicates.
918
919 **Fig. 3: M directly interacts with P via its N-terminal region and OD. A.** Scheme
920 of the secondary structure of P protein (α_{N1}, α_{N2}, α_{C1} and α_{C2} denote transient helices
921 detected in isolated P (35)) and the P constructs used. $P_{1\text{-}163}$ and $P_{1\text{-}161}$ constructs
922 were used for bacterial and mammalian expression, respectively. **B.** SDS-PAGE and
923 Coomassie blue staining of purified recombinant M, P and P fragments. **C.** M protein
924 was co-incubated with P or P fragments for 30 min prior analysis of formation of
925 complexes by band shift on native agarose gel. Arrows indicate complex formation.
926 **D.** BEAS-2B cells were co-transfected with pcDNA3.1 plasmids expressing RSV M,
927 F, N, and P WT or P deletion mutants. Cells were fixed, and immunostained with
928 anti-M (green) and anti-P (red) antibodies followed by Alexa Fluor secondary

929 antibodies, and were analyzed by confocal microscopy**.** Scale bars represent 10µm.
930 Merged images are zoomed in 3X.
931
932 **Fig. 4: Observation of a direct interaction between RSV P1-163 and M-Y229A**
933 **mutant by NMR. A.** Superimposed 2D ^{1}H-^{15}N BEST-TROSY HSQC spectra and **B.** 1D
934 ^{1}H spectra with water suppression of 25 µM ^{15}N-labeled P_{1-163} alone (red) and with 4
935 molar equivalents of M-Y229A (black). Acquisition was done in 50 mM Na phosphate
936 pH 6.7, 150 mM NaCl buffer at 800 MHz ^{1}H frequency and a temperature of 288 K.
937 Residue-specific assignment of each 2D peak is indicated by the P residue number and
938 the amino acid type. Signals with significant intensity decrease are annotated in colour.
939 Arrows indicate specific M ^{1}H NMR signals, in methyl (-1-1 ppm) and aromatic (6-7
940 ppm) proton regions. **C**. Intensity ratios (I/I_0), represented as bar diagrams, were
941 measured for each peak in the HSQC spectra of 25 µM ^{15}N-labeled P_{1-163} in the
942 absence and in presence of M-Y229A, at P:M molar ratios of 1:2 and 1:4. Signals from
943 the α-helical oligomerization domain (α_{OD}, hatched area) are broadened beyond
944 detection. Coloured background indicates the localization of P specific regions:
945 transient helices α_{N1}, α_{N2} (also termed site I), extended region β_N and site II upstream of
946 α_{OD}. **D.** Intensity ratios (I/I_0) measured from HSQC spectra of 40 µM P_{1-163} in the
947 absence and in the presence of 150 µM M-Y229A, using two different salt
948 concentrations, 150 mM and 300 mM, as indicated.
949
950 **Fig. 5: Localisation of RSV M-Y229A interaction regions on P by NMR using**
951 **fragments of P_{1-163}.** Superimposed 2D ^{1}H-^{15}N BEST-TROSY HSQC spectra of ^{15}N-
952 labeled N-terminal P fragments. Samples were in 50 mM Na phosphate pH 6.7 150
953 mM NaCl buffer. Spectra were recorded at 800 MHz ^{1}H frequency. **A.** 25 µM ^{15}N-

954 labeled P_{1-126} alone (green) and after addition of 4 molar equivalents of M-Y229A
955 (black) at a temperature of 288 K, **B.** 50 µM ^{15}N-labeled $P_{113-163}$ alone (pink) and with
956 2 molar equivalents of M-Y229A (black), at 288 K and 298 K, **C.** 25 µM ^{15}N-labeled
957 $P_{120-160}$ alone (blue) and in the presence of 2 molar equivalents of M-Y229A (black),
958 at 288 K. **D.** Intensity ratios (I/I_0) were determined from the HSQC spectra of P_{1-126}
959 and $P_{113-163}$ with and without M-Y229A. Signals from the OD (α_{OD}, hatched area),
960 which are broadened beyond detection at 288K for $P_{113-163}$, become visible at 298 K.
961 Other areas are highlighted using the same colour code as in Fig. 4.
962
963 **Fig. 6: Validation of novel M-binding sites on P using P deletion mutants. A.**
964 Scheme of the P protein secondary structure and the P constructs used. **B.** His-
965 tagged and size-exclusion chromatography purified M, P or P fragments purified on
966 glutathione beads were analysed using SDS-PAGE and Coomassie Blue staining. **C.**
967 Purified M WT (upper panel) or M Y229A (lower panel), and P or P deletion
968 constructs were incubated 30 min prior analysis of formation of complexes by band
969 shift on native agarose gel. Arrows indicate complex formation. **D.** 293T cells were
970 transfected with pairs of M and P constructs fused to 114 or 11S NanoLUC subunit,
971 combined as shown in the graph. P/P was used as positive control. Cells were lysed
972 24 h post transfection, and luminescence was measured using a Tecan Infinite 200
973 plate reader. The NLR is the ratio between actual read and negative controls (each
974 protein with the empty NanoLUC vector). The graph is representative of four
975 independent experiments, each done in three technical repeats. Data represents the
976 means and error bars represent standard deviation across 4 independent biological
977 replicates.

978 *p<0.05 (unpaired two-tailed t-test). **E.** Same cellular lysates used in D. were then
979 subjected to Western analysis using anti-P or anti-M polyclonal antibody. Size
980 markers are shown on the left side of each gel.
981
982 **Fig. 7: Functional analysis of P regions displaying direct M-binding. A.** Scheme
983 of the P protein secondary structure and the P constructs used. **B.** BEAS-2B cells
984 were co-transfected with pcDNA3.1 plasmids expressing RSV M, N, F and P deletion
985 mutants. Cells were fixed, permeabilized at 24 h post transfection, immunostained
986 with anti-M and anti-P primary antibodies followed by Alexa Fluor secondary
987 antibodies, and were analysed by confocal microscopy**.** Scale bars represent 10 µm.
988 Merged images are zoomed in 3X. **C.** HEp-2 cells were co-transfected with
989 pcDNA3.1 plasmids expressing RSV M, F and P_{WT} (lane 1, positive control) or
990 pcDNA3.1 plasmids carrying RSV M, F and an empty pcDNA3.1 vector (lane 2,
991 negative control) or with the indicated RSV P mutant constructs (lanes 3 to 8). At 48
992 h post transfection, VLPs (top) were isolated from the supernatant by pelleting of the
993 clean supernatant through a sucrose cushion. Cell lysates (bottom) were generated
994 using RIPA buffer. VLPs and cell lysates were then subjected to Western analysis
995 using anti-P or anti-M polyclonal antibody. The amount of M and P protein in VLPs
996 was quantified using the ImageJ software, and is presented as percentage (%) of M
997 and P protein released when P_{WT} was used (100%). The graph is representative of
998 four independent experiments. Data represents the % means and error bars
999 represent standard deviation across 4 independent biological replicates. ***p<0.0001
1000 (unpaired two tailed t-test)
1001

1002 **Fig. 8: Sequence alignment of the central part of *Pneumoviridae***
1003 **phosphoproteins.** Sequence alignment for human (strains A and B), bovine and
1004 ovine respiratory syncytial virus, murine pneumonia virus, human and avian
1005 metapneumovirus P proteins was generated using T-coffee suite of program (58).
1006 Uniprot accession numbers are indicated next to each sequence and residue
1007 numbers are given for each sequence. Complete conservation is indicated with a
1008 white font on red background, and relative conservation is indicated by a red font.
1009 Conserved motifs and structure elements are annotated for hRSV P and boxed
1010 throughout the aligned sequences. The boundaries of the OD are from the cryo-EM
1011 structures of L-P complexes of hRSV and hMPV (32, 59). The “RVxF”-like motif that
1012 binds PP1 and the α_{N2} M2-1 binding site (41) are boxed in green and magenta,
1013 respectively. M binding sites I and M binding site II, as identified by NMR, are
1014 indicated or boxed in blue, respectively. Identified phosphorylation sites in the hRSV
1015 P (43, 54) are indicated by a star above the sequence.
1016

Fig. 1A

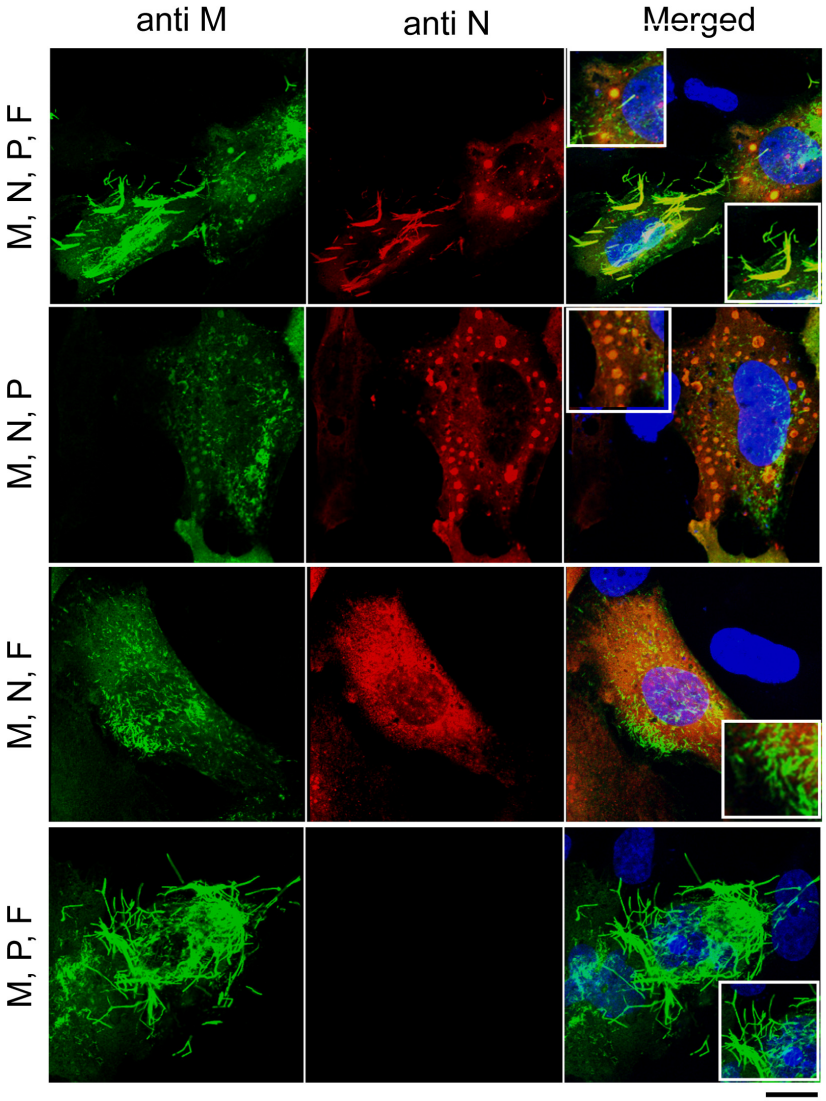

Fig. 1B

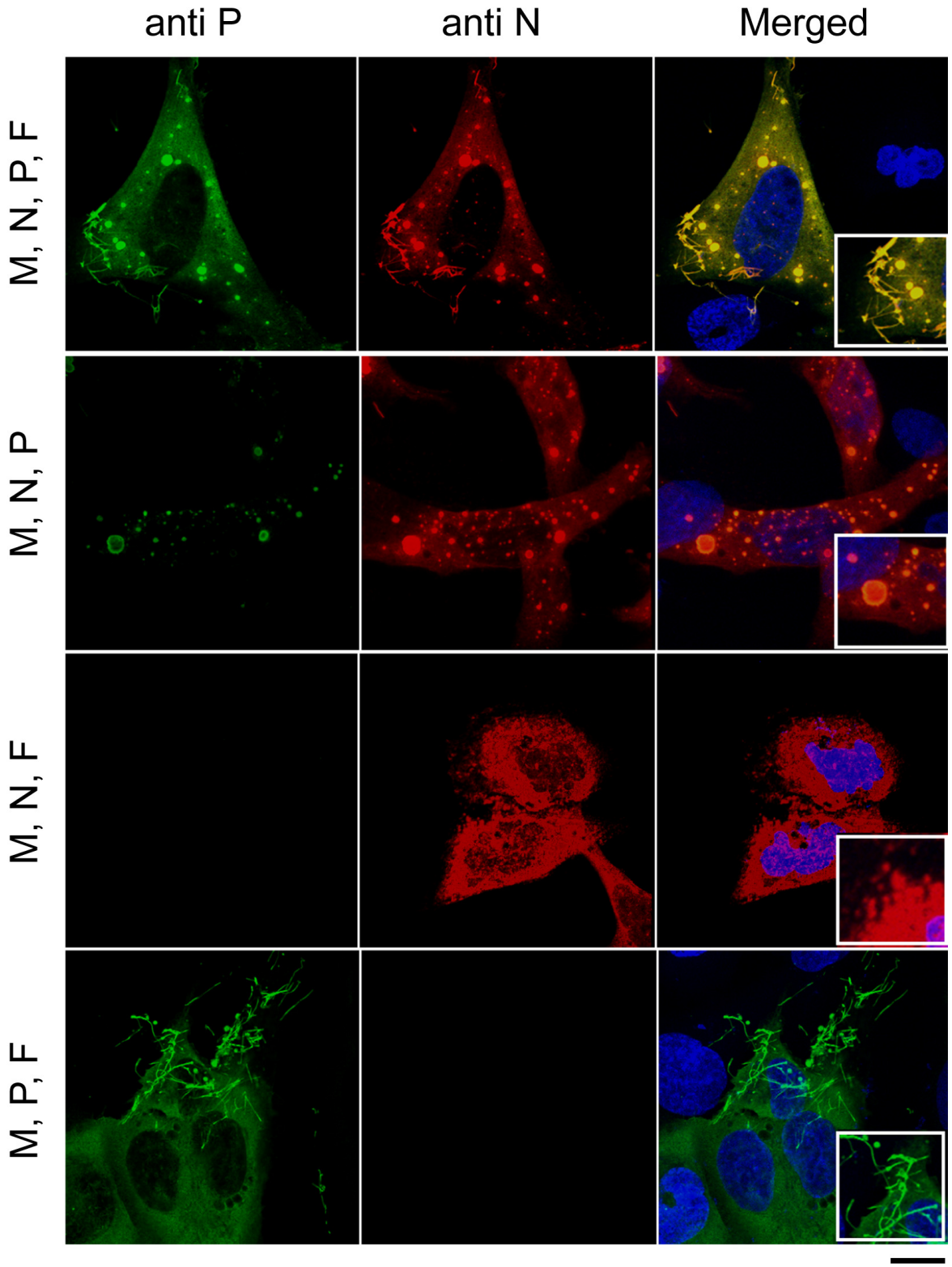

Fig. 2

A.

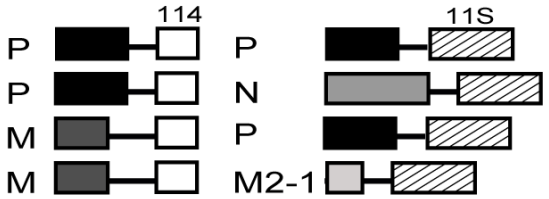

B.

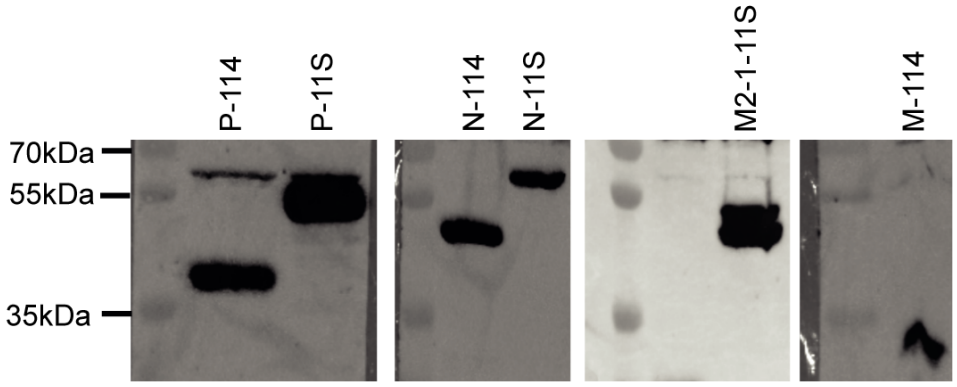

C.

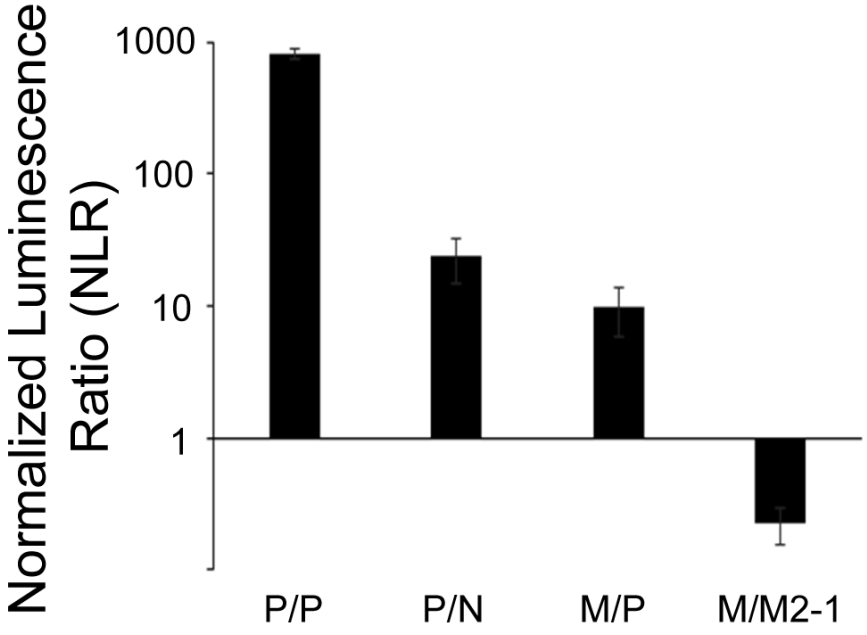

Fig. 3

A.

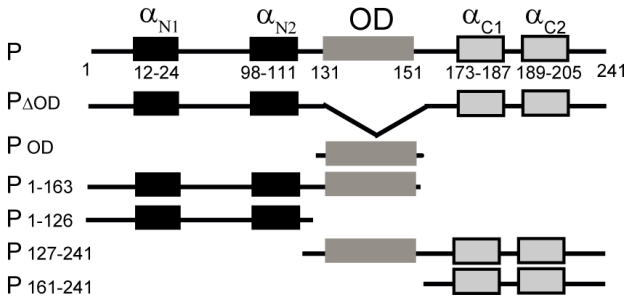

B.

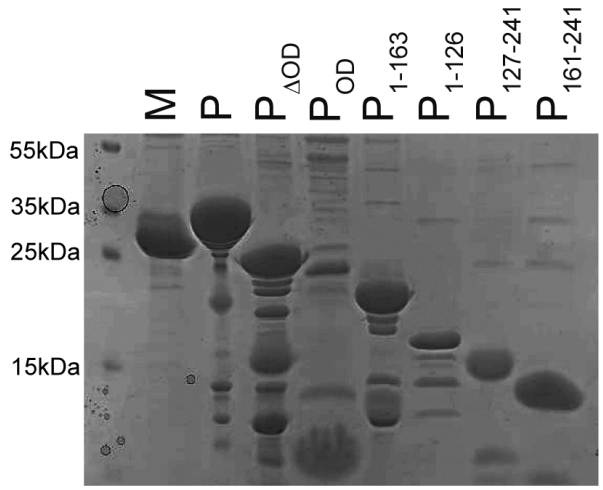

C.

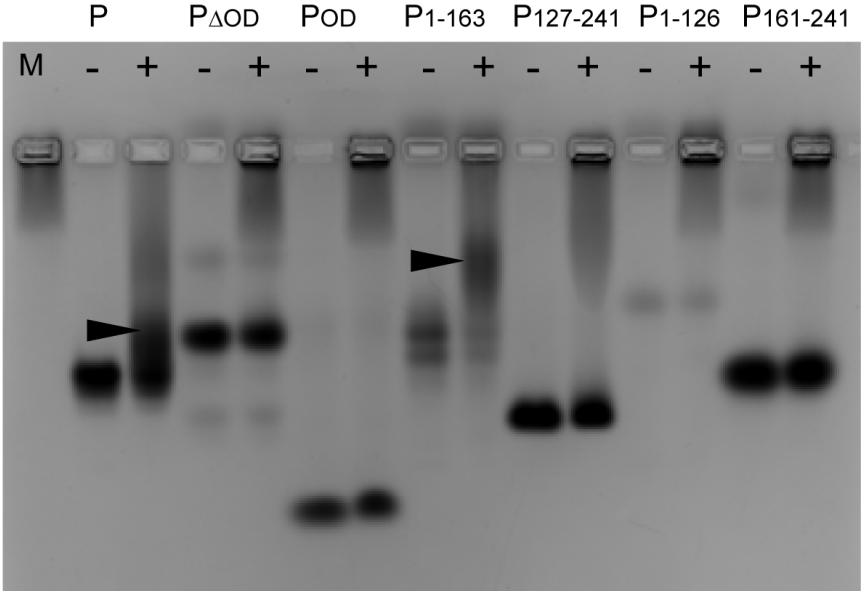

Journal of Virology

JVI

Journal of Virology

Fig. 3D

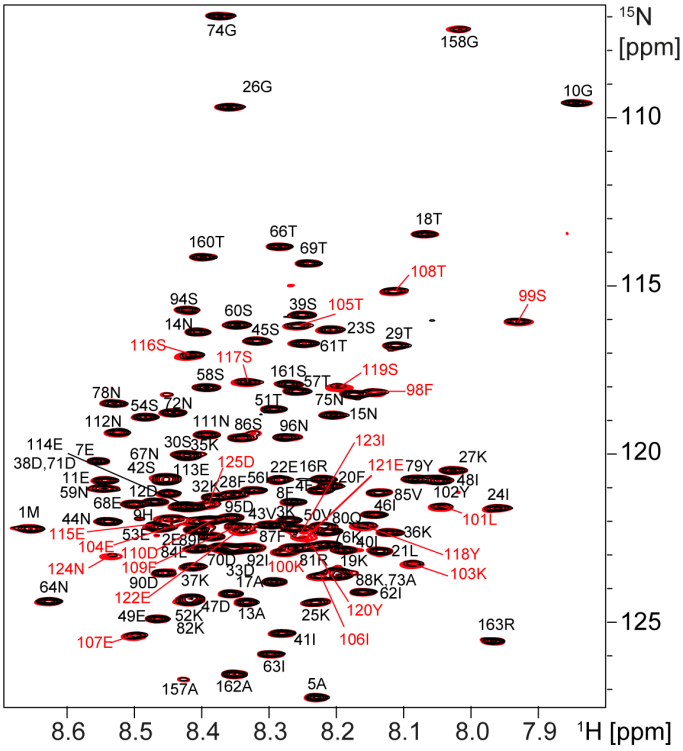

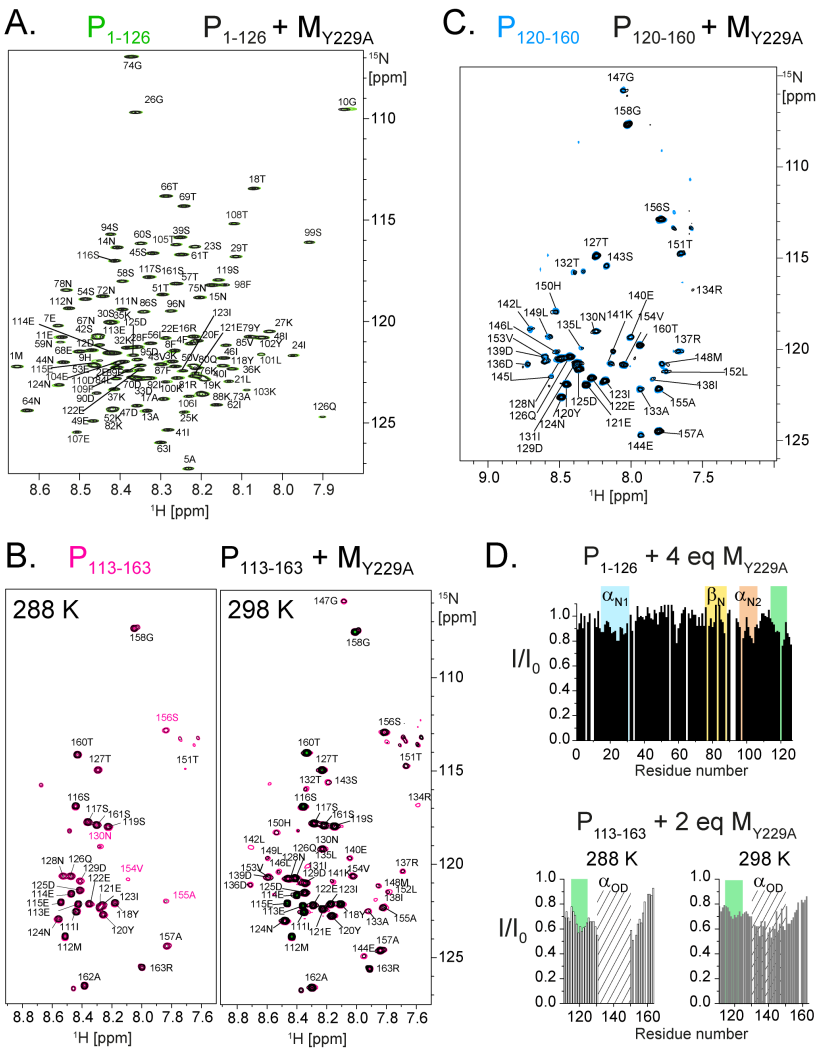

Fig. 6

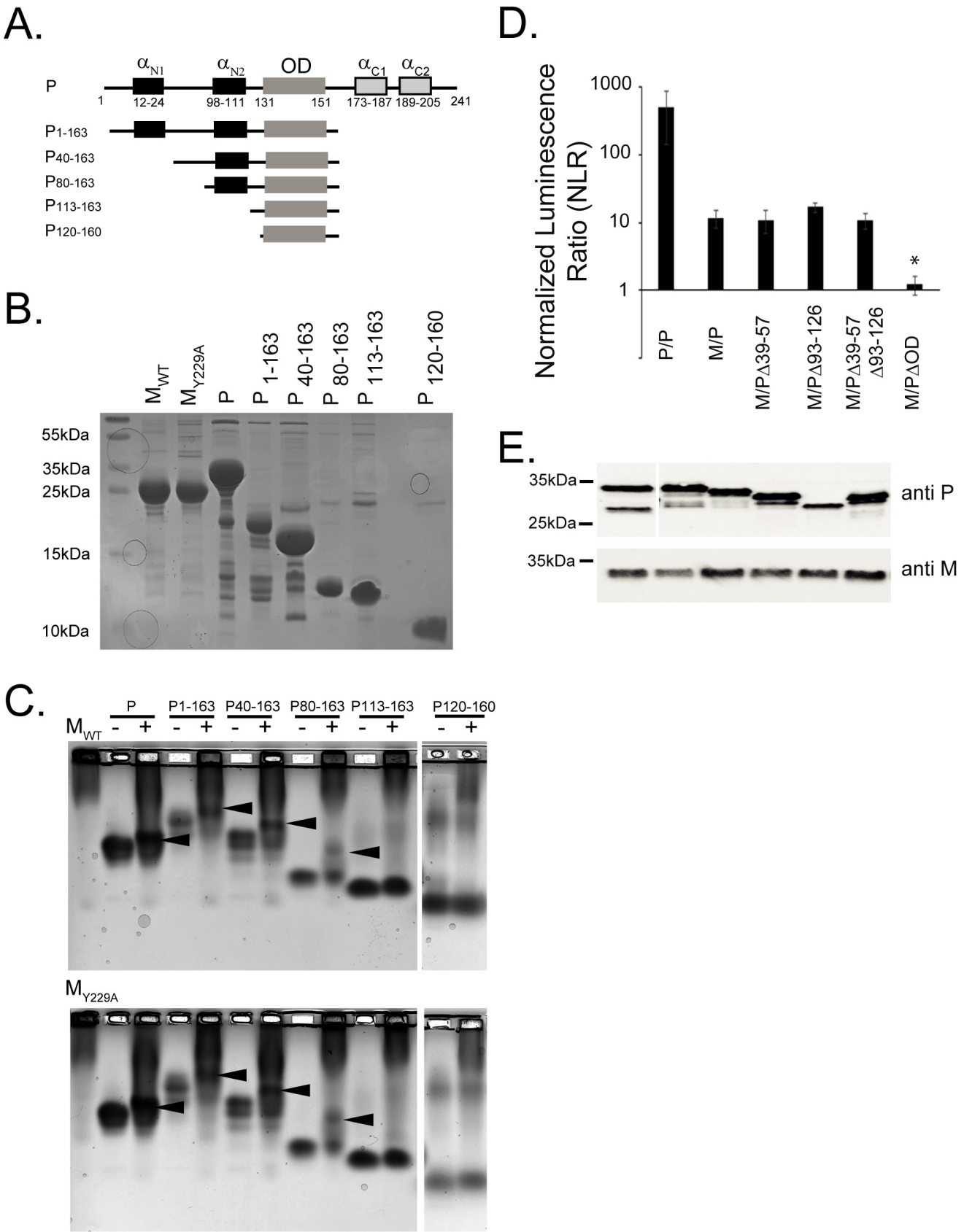

Fig. 7

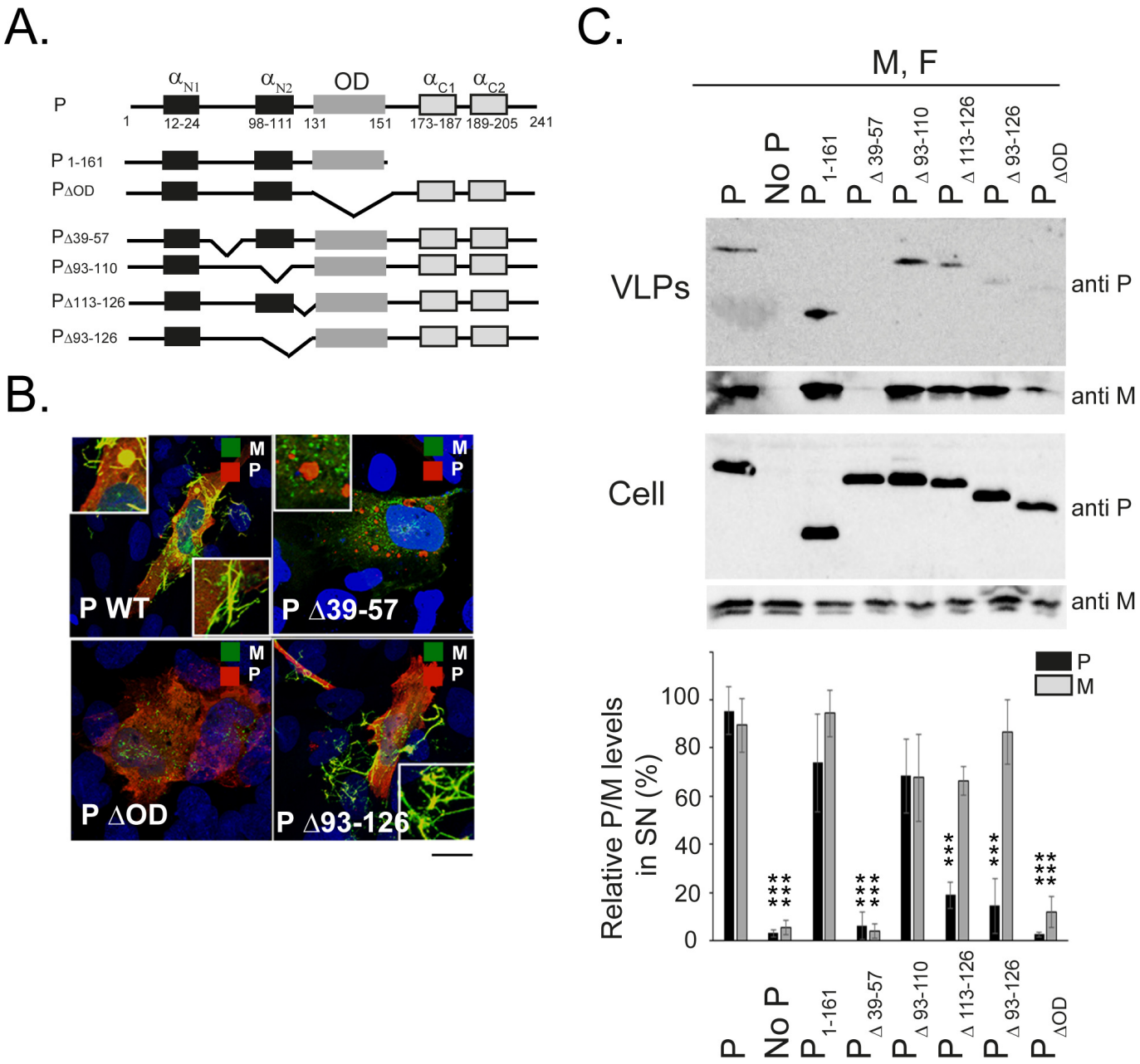

Fig. 8